Structure promoted electrochemical behavior and chemical stability of AgI-doped solid electrolyte in sulfide glass system

Baochen Ma, Qing Jiao, Yeting Zhang, Changgui Lin, Xianghua Zhang, Hongli Ma, Shixun Dai

Structure promoted electrochemical behavior and chemical stability of AgI-doped solid electrolyte in sulfide glass system

Baochen Ma[1], Qing Jiao[1*], Yeting Zhang[1], Changgui Lin[1], Xianghua Zhang[2], Hongli Ma[2], Shixun Dai[1]

[1] Laboratory of Infrared Material and Devices, Advanced Technology Research Institute, Ningbo University, Ningbo, Zhejiang, 315211, China
[2] Laboratory of Glasses and Ceramics, Institute of Chemical Science, UMR CNRS 6226, University of Rennes 1, Rennes, France

Keywords: Sulfide solid electrolyte, Electrochemical behavior, Chemical stability, AC impedances spectroscopy

ABSTRACT

Ion-conducting chalcogenide glass is a promising solid electrolyte with excellent conductivity and energy density for all-solid-state batteries. A suitable ionic channel for carriers in the amorphous network is urgently needed. In this work, the structural evolution of co-doped metal cations (Ge and Ga) in the glass matrix and its influence on electrochemical behavior was studied using a series of $Ge_xGa_{16-x}Sb_{64}S_{128}$–40AgI glass samples. The macroscopic properties of samples were examined by X-ray diffraction (XRD), differential scanning calorimetry (DSC) and Raman tests. The electrochemical behavior of samples was investigated by AC impendence spectroscopy and cyclic voltammetry (CV) measurement. Furthermore, a deliquescence experiment was applied for the chemical stability test of glass samples. The ionic conductivity of samples was developed by adding a Ga component. Notably, the electrochemical window of electrolytes was remarkably wide at approximately 5 V. The resistance of samples to humidity was characterized by the decreased Raman peaks. Analysis results show that the Ga-related bonding structure evident increased the chemical stability compared with the non-Ga sample. This work provides an insight into the effective and stable ions transport, especially in the Ge(Ga)SbS glass system. These results promote the further investigation of sulfide solid electrolytes and practical application of all-solid-state batteries.

1. Introduction

The growing demand for enhanced electrical and safety performance

in the next revolution of rechargeable batteries has promoted the rapid development of all-solid-state electrolytes[1-6]. The metal-doped chalcogenide glass, one of the potential solid electrolytes, has attracted considerable attention owing to its excellent ambient ionic conductivity and wide electrochemical window[7-11]. Using the vacuum melting technology or ball milling method, an inorganic material devoid of safety hazards, such as leakage, fire, and explosion risk, is favorable for assembling glassy electrolytes. Thus, significant progress in metal-doped glass, such as Li^+, Na^+, and Ag^+, has been made in chalcogenide system in recent years. In particular, larger halides lead to a more open network and the greater polarizability of these anions should allow for enhanced carriers diffusion. The metal halide, such as XI (X = Li, Na, Ag), is usually introduced into the glass network to ensure high ionic conductivity[12]. In 1950s, the AgI-doped solid-state battery was first studied, which facilitated the research on Ag salt-based cells (e.g., $Ag|AgI|I_2$). The solid electrolyte presented poor electrical capability with low discharge currents and an open-circuit voltage of less than 1 V. The milestone of sulfide silver superionic conductor with low E_a of 0.07 eV was illustrated by Lin et al. in 2018, where AgI up to 70 mol% can be introduced into the GeSbS system. Homogeneous glass of $2.5GeS_2$–$27.5Sb_2S_3$–70AgI presents an excellent conductivity close to commercially available electrolytes at ambient temperature[13]. Thereafter, an impressive breakthrough in the GaSbS system was achieved by Huang et al., who proved that an ionic conductivity is one order of magnitude lower than that of $Li_{10}GeP_2S_{12}$ and can be obtained from the $40(0.2Ga_2S_3–0.8Sb_2S_3)$–60AgI glass system.

Despite the excellent ionic conductivity in GeSbS and GaSbS glass systems, the difference in ion migration mechanism between them is still ambiguous. This situation impedes the deeper exploration of sulfide silver glass with better network structure. Apart from the challenge in developing ionic channels for ion migration, chemistry stability of sulfur-based solid electrolytes is another challenge[14-16]. This defect leads to a series of environmental issues (e.g., H_2S release) and makes their extensive use questionable.

In this work, AgI in a $Ge_xGa_{16-x}Sb_{64}S_{128}$ glass system was prepared and evaluated for the first time. Electrochemical measurement (using AC impedance method and CV measurement) and chemical stability test (mainly H_2O attacks) were conducted for the evolution on ionic channels and air-slaking problem. This work aims to confirm the functions of metallic element Ge or Ga in regulating the ionic conducting performance and stability with respect to different compositions. Thus, additional technologies, namely, XRD, DSC, and Raman spectra, were applied to analyze the microscopic structural evolution of samples. The insight revolution of electrochemical performance and moisture stability induced by the addition of element Ge or Ga was proposed in this work.

2. Experimental

Glass samples composed of $Ge_xGa_{16-x}Sb_{64}S_{128}$–40AgI ($0 \leq x \leq 16$ mol%) were successfully prepared by conventional melt quenching method. High-purity materials, namely, Ge, Ga, Sb, S, and AgI compounds, of a weight of approximately 10 g were mixed proportionally in a vacuum quartz ampule and heated to 900 °C for 12 h in a rocking furnace. Then, the melt was quenched and annealed at 20 °C below the glass transition temperature (T_g) for approximately 5 h. The obtained rod-like glass was processed into discs of 10 mm diameter and 2 mm thickness. The surface of both sides of a sample was polished optically and then sputtered with Au for electrochemical tests, including EIS for total resistance and CV measurement for electrochemical window. XRD was performed using Bruker D2 Phaser (10 mA, 30 kV, Cu Kα) to identify the amorphous characteristic of samples. DSC profiles were recorded on TA Q2000 work station with a scan rate of 10 °C/min. Structural evolution of glass network was illustrated by Raman spectra with Renishaw In Via (Ar ion laser 785 nm).

3. Results and discussion

3.1 Macroscopic properties

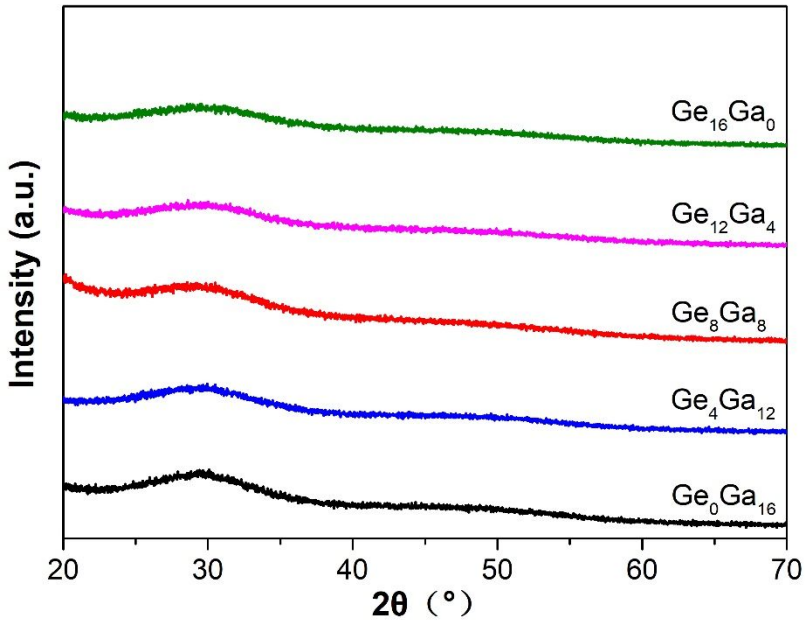

Fig. 1. Powder XRD patterns of $Ge_xGa_{16-x}Sb_{64}S_{128}$–40AgI samples.

As shown in Fig. 1, a representative XRD of obtained glass samples exhibited a broad halo peak, which indicates that all the samples are in fully amorphous nature. Thus, the excellent properties of Ge(Ga)SbS chalcogenide glass, including homogeneity, stable network structure and flexible processing characteristic, were retained in the as-prepared samples. Notably, high ionic conductivity could be easily realized in amorphous electrolytes because of the isotropic conduction pathways and lack of grain boundary resistance.

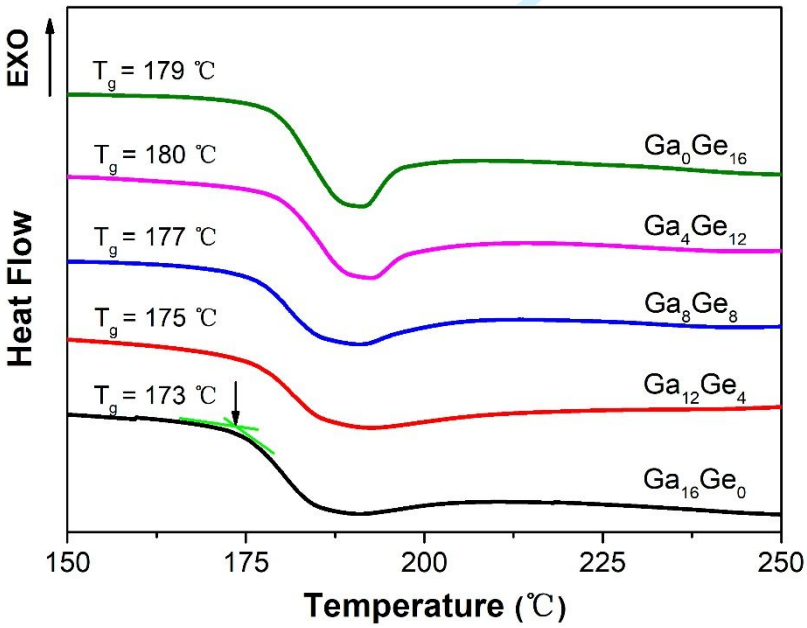

Fig. 2. DSC curves of as-prepared samples under nitrogen atmosphere.

The T_g value of the obtained glass samples verified by DSC

measurement is presented in Fig. 2. The increasing trend of T_g is related to the enlarged operating temperature range of the samples that was promoted by the substitution of Ga [Ga–S (294 kJ/mol)] by the Ge [Ge–S (265 kJ/mol)] element. However, the change in T_g was not evident among the samples, and the maximum difference was approximately 7 °C, which can be explained by the similar structural framework of the tetrahedral [GaS_4] and [GeS_4] units in the glass network.

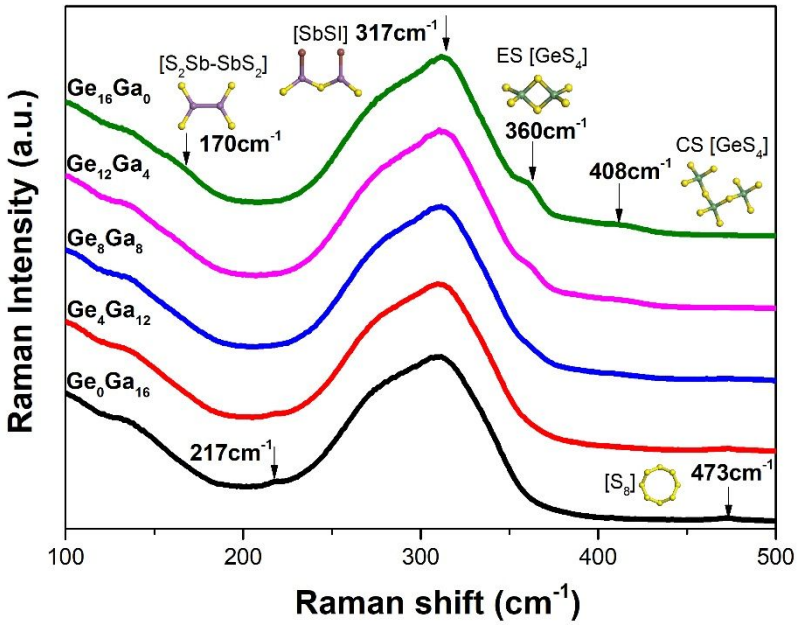

Fig. 3. Raman spectra of $Ge_xGa_{16-x}Sb_{64}S_{128}$–40AgI samples normalized by the maximum intensity of Raman peak.

Raman spectra (unitization processing) of the glass samples were studied here as a useful probe, which is sensitive to local structure and coordination in glass. As shown in Fig. 3, the most intense Raman peak located at 317 cm^{-1} was ascribed to the vibrational [SbSI] units, which indicates a major connection of the glass network. The increasing peak at 360 and 408 cm^{-1} was due to stretching vibration of edge-shared (ES) and corned-shared (CS) [GeS_4] tetrahedral units. In general, Ge prefers to form CS tetrahedra unit than the ES. However, the stronger peak of ES tetrahedra observed from Raman spectra clearly reveals the phenomenon of S deficiency in the network. At the same time, the bond vibrations devoted to 473 and 217 cm^{-1}, which were characterized by S_8 rings, were generally disappeared with the increasing addition of Ge. It is because that the aliovalent cation substitution of Ge^{4+} into the GaSbS sulfide

system (Ga^{3+}) leads to additional occupation of covalent bonds related to sulfur ions. The slight increase in Raman peak at 170 cm^{-1} related to the metallic bond of [Sb–Sb] was observed, which was in agreement with the sulfur-deficient conditions caused by addition of Ge. Interestingly, the [SbSI] band at 314 cm^{-1} in sample with higher Ge concentration was stronger than that of lower Ge concentration. It is anticipated that a large number of S^{2-} ions were coordinated with the additional Ge^{4+}, while the I^- as negative charge formed the [Sb–I] bond to compensate the sulfur-deficient condition, that is, the formation of [SbS_xI_{3-x}] units was promoted by the replacement of Ga with Ge element. Therefore, the large radius and highly-polarizable I^- ions was involved in the formation of glass network leading to a bigger and looser channel for ions' migration[17-20].

3.2. Electrochemical behavior

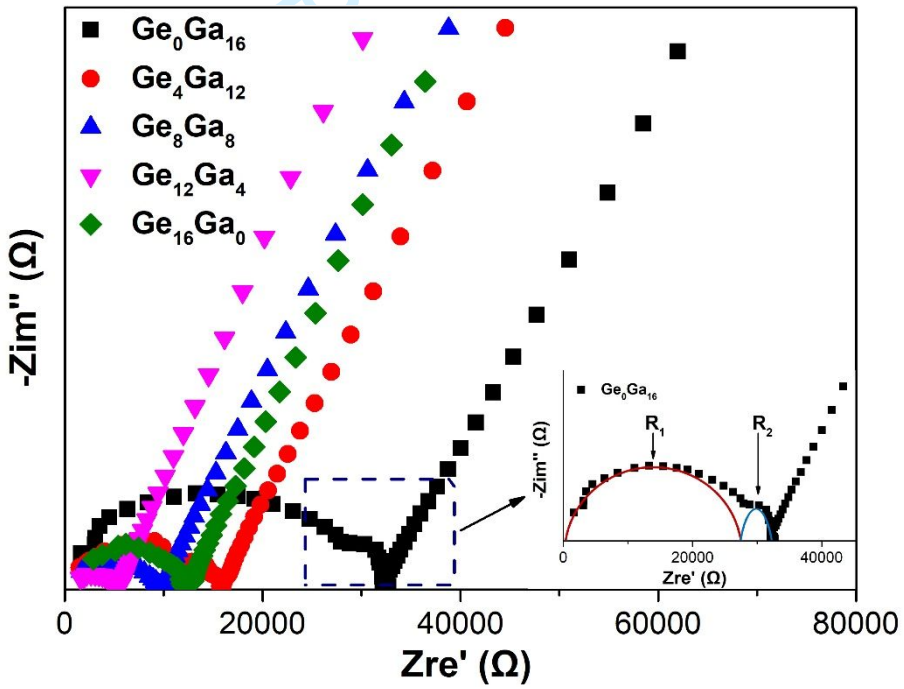

Fig. 4. Typical Nyquist plot of ionic conductor of $Ge_xGa_{16-x}Sb_{64}S_{128}$–40AgI bulk samples. The inset presents a magnified image of Ge_0Ga_{16} sample.

AC impedance measurement was performed to explore the bulk resistance of the glass samples. The Nyquist plot illustrating the variation of the total electrical and ionic conductivity at room temperature is displayed in Fig. 4. *Zre'* and *-Zim''* represent the resistance and reactance of bulk-samples, respectively. The presence of a semicircle and a spike,

which indicates a typical behavior of an ionic conductor, was observed in the higher- and lower-frequency regions of current. However, two distorted semicircles occurred in the high-frequency of Ge_0Ga_{16} sample, as shown in the inset. The resistances of bulk sample could be attributed to R_1 without any doubt. And the rest semicircle of R_2 was related to the resistances of working electrode except for the diffusion resistance of carriers, which was produced by the poor quality of the electrical contacts between electrode and electrolyte[21]. Thus, the total bulk resistance R_1 equivalent to the sum of R_e (electrical resistance) and R_i (ionic conductivity) of samples could be derived from the cross section of the arc and tail on the *x*-axis[22]. Evidently, the arcs exhibited a consistent trend, except for the $Ge_{16}Ga_0$ sample with a radius of semicircles that decreased with the increase in Ge content. The reason is that high conductivity was obtained with larger and looser ionic channels established by $[SbS_xI_{3-x}]$ units. Interestingly, the $Ge_{16}Ga_0$ bulk sample, which was supposed to have the best electrochemical behavior among the samples, presented a lower conductivity than $Ge_{12}Ga_4$. No extra characteristic peak of structural unit and additional grain boundary resistance of crystalline phase was detected by Raman spectra and XRD measurement. When the intermediate of Ga element was added, normally the ionic conductivity increases due to the weakened interaction with carriers. Therefore, the lack of Ga element, i.e. mixed-cation effect, in the ionic channels probably impedes the further improvement in ionic conductivity. That is, an effective transport channel of carriers in this work, such as $[S_3Ga–X…X–GeS_4]$ (X represents antimonide), was established not only by the single former of the Ge element but also by the diversified modifier of the Ga element.

The total conductivity was evaluated using the following equation: $\sigma_t = D/(A*R_1)$, where D is the sample thickness and A represents the gold-coated area on the interface of bulk samples. The room-temperature conductivity increased from 1.07×10^{-5} S/cm to 6.63×10^{-5} S/cm with the substitution of Ga by the Ge atom, which is consistent with the Raman and impedance analysis. The ionic conductivity of the samples presents good fitting according to the Arrhenius Law, $\sigma = \sigma_0/T\ exp(-E_a/kT)$, which

is always presented in a linear form, $\ln\sigma T = \ln\sigma_0 - E_a/kT$. σ_0 is the pre-exponential factor, E_a represents the activation energy, and k and T are the Boltzmann constant and the current temperature, respectively.

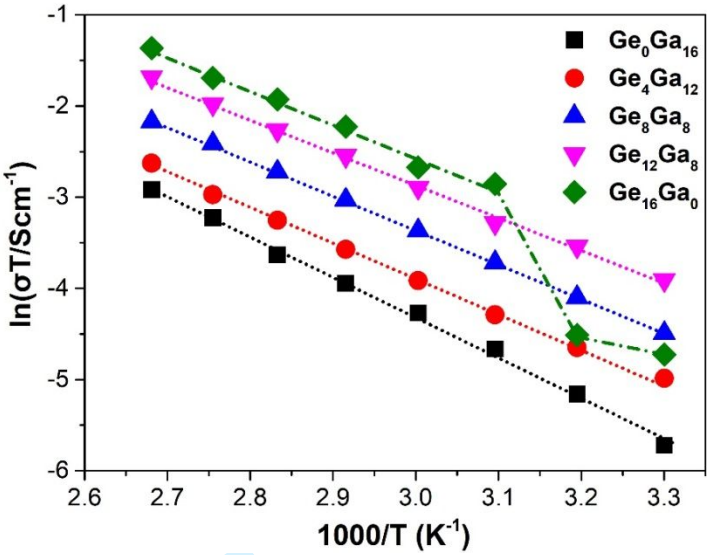

Fig. 5. Arrhenius plot with linear fitting for the bulk samples.

The temperature dependence of R_1, which is the thermally activated mobility of the carriers of samples, is demonstrated in Fig. 5. E_a corresponds to the binding energy during ion migration and is calculated from the slope of the fitting straight-line. E_a decreased from 0.38 eV to 0.31 eV with the replacement of Ga. The conductive value of the $Ge_{16}Ga_0$ sample showed a sudden leap from 10^{-5} S/cm to 10^{-4} S/cm at around 60 °C. This abrupt change in conductivity was connected with the specific thermal activation effect in the network, which possibly was produced by phase separation of glass former (Ge and Sb tetrahedron) and dopant ions (Ag^+) causing the high migration energy. When the temperature reaches 60 °C, the vibration of Ag^+ was aggravated by the heat treatment and the activated Ag ions preferred to jump from one interstitial site to another near site. Therefore, the addition of Ga in the glass network, to some extent, restrains the phase separation and improves the room-temperature conductivity compared with the Ge single-doped sample.

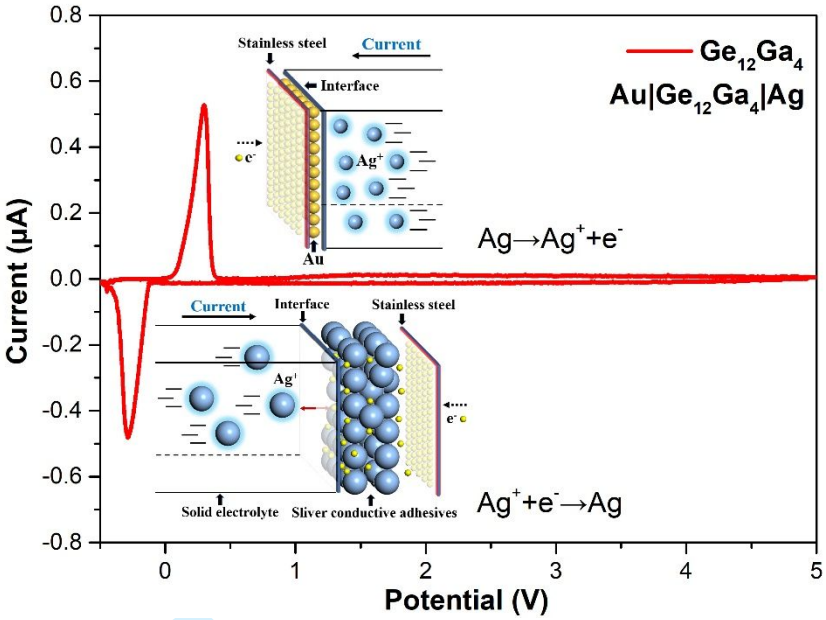

Fig. 6. Cyclic voltammetry of $Ge_{12}Ga_4$ sample with an Au|$Ge_{12}Ga_4Sb_{64}S_{128}$–40AgI|Ag cell from −0.5 V to 5 V.

The electrochemical stability of the $Ge_{12}Ga_4$ sample against metallic silver was measured through CV test using a Au|$Ge_{12}Ga_4$|Ag cell, as displayed in Fig. 6. The potential was scanned from −0.5 V to 5 V versus Ag/Ag^+ at a scanning rate of 5 mV/s. Obviously, no peak characterized by the extra redox reactions was observed up to 5 V, except for two sharp peaks responsible for silver dissolution and deposition in the low-voltage region. This phenomenon demonstrates that a stable and broad electrochemical window was obtained from the present sample[23-25]. The detailed anodic and cathodic reactions near 0 V were explained by the schematic of the atomic simulation, as shown in the insets of Fig. 6. The silver element (marked by blue balls) distributed in the anode lost electrons (marked by little yellow balls) and moved toward the cathode when a positive voltage was applied in the cell. By contrast, when negative voltage was applied, the sliver ions (marked by shinning blue balls) assembling around the cathode of Au (marked by golden balls) returned to the anode and combined with the electrons. Consequently, the two equal integral areas near 0 V, which illustrate the formation of an effective and reliable ionic transport mechanism in the network, are responsible for the higher conductivity and lower activation energy than those of the other samples.

3.3. Chemical stability

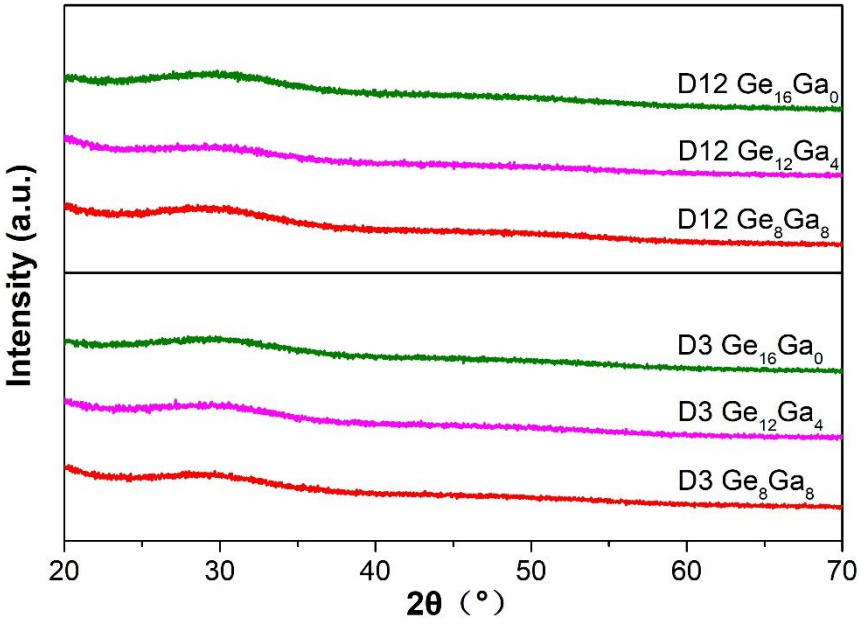

Fig. 7. Powder XRD patterns of $Ge_xGa_{16-x}Sb_{64}S_{128}$–40AgI (x = 8, 12, 16) samples after 3- and 12-days exposure.

In air, chalcogenide glass electrolytes show deliquescence and hydrolysis reaction with moisture, which weaken the electrochemical performance and result in safety problem if not properly addressed. The processability in air and high tolerance to moisture of sulfide solid electrolyte are significant factors that influence the practical applications. Given that one of the primary problems with sulfide materials is their poor chemical stability, the investigation of the chemical stability of Ge_xGa_{16-x} glass (x = 8, 12, 16) is necessary for their further improvement and application. Therefore, the Ge_xGa_{16-x} glass powder was exposed to humidity for 3 days (D3) and 12 days (D12) at room temperature. The corresponding phase change was measured by XRD. According to the XRD pattern shown in Fig. 7, no distinct crystalline peak was observed in the D3 or D12. This finding proves that the current samples were remarkably resistant to devitrification under moisture attack and remained in a stable amorphous state. Meanwhile, the detailed micro-structural changes of glass related to ionic channels were observed from the Raman spectra for D3 and D12, as plotted in Fig. 8.

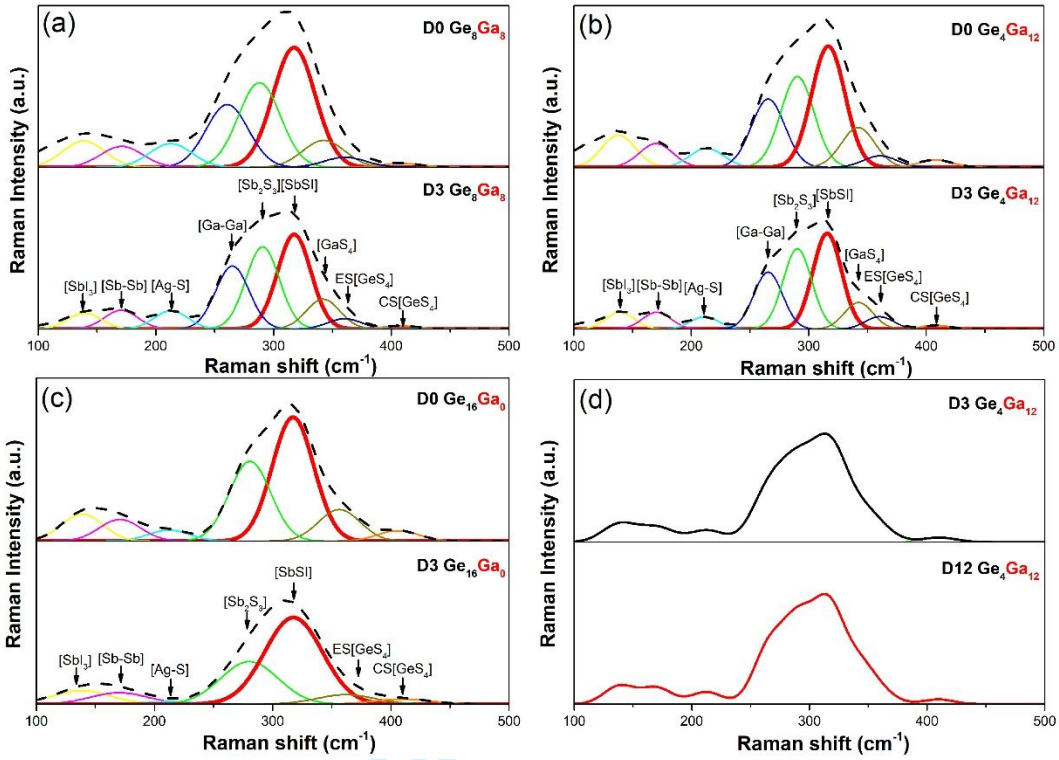

Fig. 8. Decomposed Raman scattering spectra of $Ge_xGa_{16-x}Sb_{64}S_{128}$–40AgI (x = 8, 12, 16) samples after 3- and 12-days exposure.

The as-prepared powder sample after the deliquescence process for different times was subjected to Raman scattering measurement for a better understanding of the influence of humidity on the network. The Raman peaks were decomposed in a series of sub-bands for further accurate analysis by Gaussian fitting method[26, 27]. Figs. 8 (a)–(c) indicate that, after three days of exposure, the entire Raman peak presented a declining trend in intensity. One of the evident changes in the glass network was ascribed to the [SbSI] and [SbI_3] units, which illustrates the unstable chemical properties of the [$SbS_{3-x}I_x$] pyramid units (x >0) in the samples. Meanwhile, the declining intensity of the peak characterized by the [S_2Sb–SbS_2] and [Sb_2S_3] units was related to the difference in composition. The damage of the Sb-related units in the Ga-doped glass sample, namely, (a) and (b), was suppressed to some extent compared with that of the sample without Ga. Meanwhile, the vibrational intensity of Ge- and Ga-related units, such as [GeS_4], [GaS_4], and [S_3Ga-GaS_3], in the samples containing Ga, decreased slightly after three days of exposure. That is, the Ga atom as a modifier in the glass network also impeded the decomposition of the tetrahedra and ethane-like

units in the network. The reason is that the monovalent glass modifiers, such as AgI, formed non-bridging sulfur (NBS) units in the network, whereas the introduction of trivalent glass intermediates, such as Ga_2S_3, eliminated the NBS units by forming a dative Ga–S bond and stabilized the network structure without serious distortion[12, 28]. Thus, the intensity of the Raman band devoted to [Ag–S] was stronger in (a) and (b) than in (c). After longer exposure, the corresponding Raman spectra of D3 and D12 samples were compared, as shown in Fig. 8 (d). The comparison shows no evident change between the D3 and D12 samples, which suggests that the glass structure was deconstructed within a short time (within 3 days). Moreover, slowing the process of electrolytes' decomposition further under the normal environment is necessary for improving their cycling performance and work life.

Therefore, the chemical stability, especially resistance to moisture, can be optimized by the addition of Ga in the glass network. Notably, the H_2S release of chalcogenide solid electrolyte with high electrochemical performance can be controlled and reduced by improving the chemical stability.

4. Conclusions

In this work, the optimized composition of the Ge(Ga)SbS sample, which has better electrochemical performance and chemical stability, was found in $Ge_{12}Ga_4$ glass. The compactness and T_g of the amorphous samples increased with Ga substitution, and an acceptable mechanical property was realized in the Ge(Ga)SbS system. The increase in conductivity of 6.63×10^{-5} S/cm was obtained from the $Ge_{12}Ga_4$ sample combined with a stable and broad electrochemical window of up to 5 V. Meanwhile, the good chemical stability of $Ge_{12}Ga_4$ was verified by a comparison test with different exposure times under humid atmosphere. Ga ions, which were used as a modifier in the network, reduced the amount of NBS units by forming [GaS_4] tetrahedron units that enhance the chemical stability. Ge ions, which acted as the glass former, enlarged the channel size by promoting the formation of [SbS_xI_{3-x}] units and contributed to the ionic conductivity. Further exploration and investigation of the Ge(Ga)SbS sulfide electrolyte system, such as

improvement in ionic conductivity, the compatibility of the electrode/electrolyte interface, and the reliability of the cycle performance, are needed to promote the commercial application of all-solid-state batteries.

Acknowledgments

This work was financially supported by National Natural Science Foundation of China (Grant no. 51972176).

Reference

[1] R. Chen, Q. Li. Approaching Practically Accessible Solid-State Batteries: Stability Issues Related to Solid Electrolytes and Interfaces, Chem Rev (2019). http://doi.org/10.1021/acs.chemrev.9b00268.

[2] N. Tanibata, M. Deguchi. All-Solid-State Na/S Batteries with a Na_3PS_4 Electrolyte Operating at Room Temperature, Chemistry of Materials 29(12) (2017) 5232-5238. http://doi.org/10.1021/acs.chemmater.7b01116.

[3] N. Tanibata, K. Noi. Preparation and characterization of Na_3PS_4–Na_4GeS_4 glass and glass-ceramic electrolytes, Solid State Ionics 320 (2018) 193-198. http://doi.org/10.1016/j.ssi.2018.02.042.

[4] B.E. Francisco, C.M. Jones. Nanostructured all-solid-state supercapacitor based on Li_2S-P_2S_5 glass-ceramic electrolyte, Applied Physics Letters 100(10) (2012). http://doi.org/10.1063/1.3693521.

[5] T.-F. Yi, Y.-M. Li. Enhanced electrochemical property of $FePO_4$-coated $LiNi_{0.5}Mn_{1.5}O_4$ as cathode materials for Li-ion battery, Science Bulletin 62(14) (2017) 1004-1010. http://doi.org/10.1016/j.scib.2017.07.003.

[6] H. Zhang, A. Rousuli, S. Shen, et al. Enhancement of superconductivity in organic-inorganic hybrid topological materials, Science Bulletin 65(3) (2020) 188-193. http://doi.org/10.1016/j.scib.2019.11.021.

[7] A. Sakuda, A. Hayashi. Metastable Materials for All-Solid-State Batteries, Electrochemistry 87(5) (2019) 247-250. http://doi.org/10.5796/electrochemistry.19-H0002.

[8] N. Kamaya, K. Homma, Y. Yamakawa, et al. A. Mitsui, A lithium superionic conductor, Nat Mater 10(9) (2011) 682-6. http://doi.org/10.1038/nmat3066.

[9] M.A.T. Marple, B.G. Aitken. Fast Li-Ion Dynamics in Stoichiometric Li_2S–Ga_2Se_3–$GeSe_2$ Glasses, Chemistry of Materials 29(20) (2017) 8704-8710. http://doi.org/10.1021/acs.chemmater.7b02858.

[10] S. Chen, X. Qiao, Z. Zheng, et al. Enhanced electrical conductivity and

photoconductive properties of Sn-doped Sb_2Se_3 crystals, Journal of Materials Chemistry C 6 (2018). http://doi.org/10.1039/C8TC01683F.

[11] M. Kaes, M. Le Gallo. High-field electrical transport in amorphous phase-change materials, Journal of Applied Physics 118(13) (2015). http://doi.org/10.1063/1.4932204.

[12] J. Lau, R.H. DeBlock. Sulfide Solid Electrolytes for Lithium Battery Applications, Advanced Energy Materials 8(27) (2018). http://doi.org/10.1002/aenm.201800933.

[13] C. Lin, E. Zhu. Fast Ag-ion-conducting GeS_2–Sb_2S_3–AgI glassy electrolytes with exceptionally low activation energy, The Journal of Physical Chemistry C 122(3) (2018) 1486-1491. http://doi.org/10.1021/acs.jpcc.7b10630.

[14] X. Li, J. Liang, J. Luo, et al. Air-stable Li_3InCl_6 electrolyte with high voltage compatibility for all-solid-state batteries, Energy & Environmental Science (2019). http://doi.org/10.1039/c9ee02311a.

[15] X. Sun, X. Li, J. Liang, et al. H_2O-Mediated Synthesis of Superionic Halide Solid Electrolyte, Angew Chem Int Ed Engl (2019). http://doi.org/10.1002/anie.201909805.

[16] S.L. Shang, Z. Yu. Origin of outstanding phase and moisture stability in $Na_3P_{1-x}As_xS_4$ superionic conductor, ACS Applied Material & Interfaces 9(19) (2017). http://doi.org/10.1021/acsami.7b03606.

[17] M. Zhang, Z. Yang, L. Li, et al. The effects of germanium addition on properties of Ga-Sb-S chalcogenide glasses, Journal of Non-Crystalline Solids 452 (2016) 114-118. http://doi.org/10.1016/j.jnoncrysol.2016.08.023.

[18] I. Pethes, V. Nazabal, J. Ari, et al. Atomic level structure of Ge-Sb-S glasses: Chemical short range order and long Sb-S bonds, Journal of Alloys and Compounds 774 (2019) 1009-1016. http://doi.org/10.1016/j.jallcom.2018.09.334.

[19] H.-T. Guo, M.-J. Zhang. Structural evolution study of additions of Sb_2S_3 and CdS into GeS_2 chalcogenide glass by Raman spectroscopy, Chinese Physics B 26(10) (2017). http://doi.org/10.1088/1674-1056/26/10/104208.

[20] Pumlianmunga, K. Ramesh. SET and RESET states of As_2Se_3 doped $GeTe_4$ bulk glasses probed by Raman spectroscopy, Journal of Applied Physics 120(21) (2016). http://doi.org/10.1063/1.4971253.

[21] D. Fasquelle, J.-C. Carru. Electrical characterizations of silver chalcogenide glasses, Journal of Non-Crystalline Solids 353(11-12) (2007) 1120-1125. http://doi.org/10.1016/j.jnoncrysol.2006.12.024.

[22] F. Tsuji, N. Tanibata. Preparation of Sodium Ion Conductive $Na_{10}GeP_2S_{12}$ Glass-ceramic Electrolytes, Chemistry Letters 47(1) (2018) 13-15. http://doi.org/10.1246/cl.170836.

[23] J. Yang, H.-L. Wan, Z.-H. Zhang, et al. NASICON-structured $Na_{3.1}Zr_{1.95}Mg_{0.05}Si_2PO_{12}$ solid electrolyte for solid-state sodium batteries, Rare Metals 37(6) (2018) 480-487. http://doi.org/10.1007/s12598-018-1020-3.

[24] L. Zhang, D. Zhang, K. Yang, et al. Vacancy-Contained Tetragonal Na_3SbS_4 Superionic Conductor, Advanced Science 3(10) (2016) 1600089. http://doi.org/10.1002/advs.201600089.

[25] A. Hayashi, K. Noi. Superionic glass-ceramic electrolytes for room-temperature rechargeable sodium batteries, Nat Commun 3 (2012) 856. http://doi.org/10.1038/ncomms1843.

[26] X. Huang, Q. Jiao. Compositional dependence of the optical properties of novel Ga-Sb-S-XI (XI = PbI_2, CsI, AgI) infrared chalcogenide glasses, Journal of the American Ceramic Society 101(2) (2018) 749-755. http://doi.org/10.1111/jace.15238.

[27] M. Fraenkl, B. Frumarova, V. Podzemna, et al. How silver influences the structure and physical properties of chalcogenide glass $(GeS_2)_{50}(Sb_2S_3)_{50}$, Journal of Non-Crystalline Solids 499 (2018) 412-419. http://doi.org/10.1016/j.jnoncrysol.2018.07.046.

[28] A. Yang, M. Zhang, L. Li, et al. Ga-Sb-S chalcogenide glasses for mid-infrared applications, Journal of the American Ceramic Society 99(1) (2016) 12-15. http://doi.org/10.1111/jace.14025.

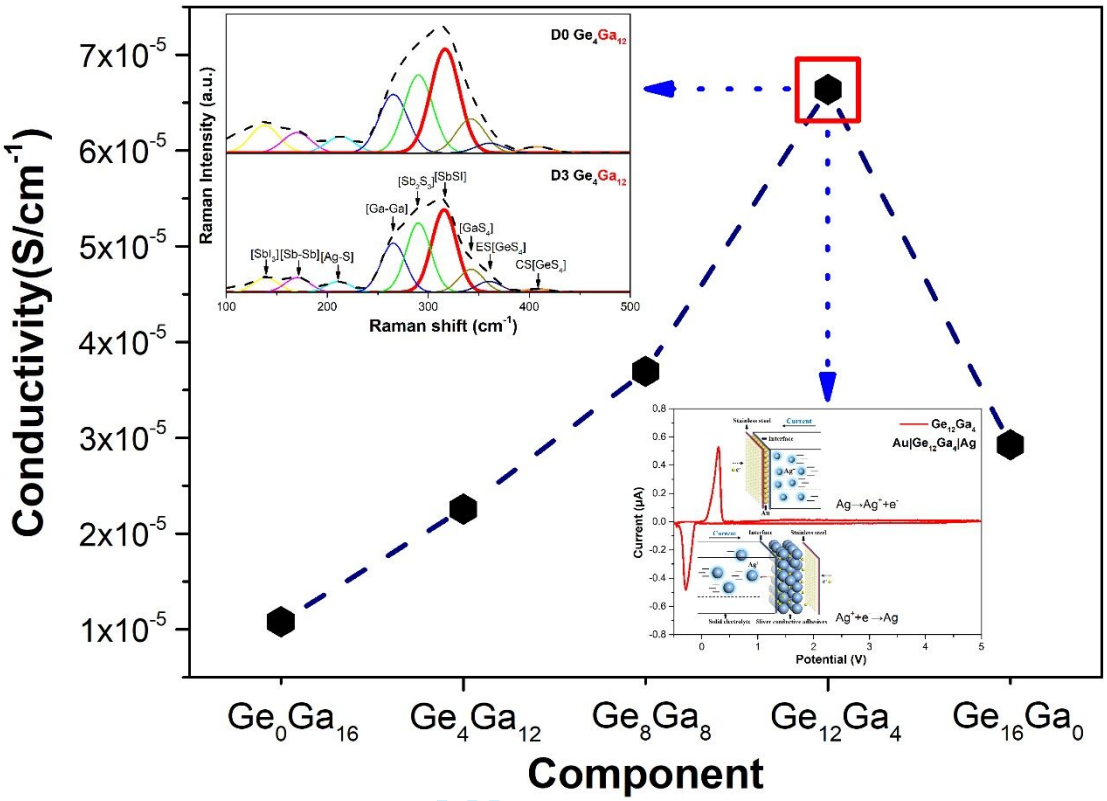

Homogeneous $Ge_xGa_{16-x}Sb_{64}S_{128}$–40AgI sulfide glass presented optimized electrochemical performance and chemical stability at x = 12.